1-1-2010

Rotor position and speed estimation of a variable structure direct-torque-controlled IPM synchronous motor drive at very low speeds including standstill

Saad M. Sayeef
University of Wollongong, saad@uow.edu.au

Gilbert Foo
University of New South Wales

Muhammad F. Rahman
University of New South Wales

Rotor position and speed estimation of a variable structure direct-torque-controlled IPM synchronous motor drive at very low speeds including standstill

Abstract

The performance of a speed sensorless variable structure direct-torque-controlled interior permanent magnet synchronous motor drive at very low speeds including standstill is investigated in this paper. The rotor position and speed are estimated using a high-frequency (HF) signal injection algorithm at low speeds and a sliding observer at medium to high speeds. The changeover between these two algorithms is performed using a weighting function which smoothly hands over the estimated rotor position information for stator flux and torque estimation purposes. Experiments were performed to test the effectiveness of the proposed HF signal injection algorithm, and results show that the sensorless drive is capable of accurately estimating the position and speed at very low speeds including standstill. The implementation of the changeover algorithm to switch between the two observers at low and high speeds has enabled sensorless operation of the drive from zero to base speed.

Keywords

Rotor, position, speed, estimation, variable, structure, direct, torque, controlled, IPM, synchronous, motor, drive, very, low, speeds, including, standstill

Disciplines

Physical Sciences and Mathematics

Publication Details

Sayeef, S. M., Foo, G. & Rahman, M. (2010). Rotor position and speed estimation of a variable structure direct-torque-controlled IPM synchronous motor drive at very low speeds including standstill. IEEE Transactions on Industrial Electronics, 57 (11), 3715-3723.

Rotor Position and Speed Estimation of a Variable Structure Direct-Torque-Controlled IPM Synchronous Motor Drive at Very Low Speeds Including Standstill

Saad Sayeef, *Member, IEEE*, Gilbert Foo, *Student Member, IEEE*, and M. F. Rahman, *Senior Member, IEEE*

***Abstract*—The performance of a speed sensorless variable structure direct-torque-controlled interior permanent magnet synchronous motor drive at very low speeds including standstill is investigated in this paper. The rotor position and speed are estimated using a high-frequency (HF) signal injection algorithm at low speeds and a sliding observer at medium to high speeds. The changeover between these two algorithms is performed using a weighting function which smoothly hands over the estimated rotor position information for stator flux and torque estimation purposes. Experiments were performed to test the effectiveness of the proposed HF signal injection algorithm, and results show that the sensorless drive is capable of accurately estimating the position and speed at very low speeds including standstill. The implementation of the changeover algorithm to switch between the two observers at low and high speeds has enabled sensorless operation of the drive from zero to base speed.**

***Index Terms*—Direct torque control (DTC), sensorless, signal injection, variable structure.**

I. Introduction

DIRECT TORQUE CONTROL (DTC) for induction motor drives was first proposed in the 1980s by Depenbrock [1] and Takahashi and Naguchi [2]. This concept was also applied to interior permanent magnet (IPM) synchronous machines (IPMSMs) in the late 1990s [3], [4].

When compared to conventional field-oriented control (FOC) drives, DTC possesses several advantages, which include the elimination of the dq-axis current controllers, the associated coordinate transformation, the rotor position sensor requirement, and the separate voltage pulsewidth modulator [5]. However, DTC has its own drawbacks, which include high torque, flux, and current ripples, variable switching frequency behavior, and difficulty to control torque and flux at a very low speed [16]. As the switching state of the inverter is updated only once in every sampling interval, this affects the control resolution, which results in higher ripples in torque and flux when compared to those of vector control drives. This problem can be solved by using multiple-level inverters [6] to generate more control voltage space vectors, thus improving control resolution to reduce torque and flux ripples. However, the increased number of power switches needed increases the system cost and complexity. Switching losses inevitably increase too, thus decreasing the system efficiency. Model predictive DTC schemes were investigated in [21] and [22] to reduce torque ripples, but these methods are significantly more complex and computationally intensive for implementation.

There is no pulsewidth modulation (PWM) involved in a DTC drive since the voltage-source inverter switching signals are directly produced by the switching policy. Another advantage of DTC over FOC is the elimination of the requirement for continuous position information as the DTC algorithm is conducted in the stationary reference frame.

DTC algorithms using space vector modulation (SVM) for IPMSMs were investigated in [5] and [7], both of which have reduced torque and flux ripples significantly, with a fixed switching frequency. The method in [5] utilizes a proportional–integral (PI) controller, and the scheme in [7] uses a variable structure controller.

The variable structure direct torque controller (VS-DTC) in [7] for IPMSM drives is modified and implemented in this paper. The reference voltage vectors are generated by the SVM unit. When compared to the classical DTC scheme, the VS-DTC method suppresses the torque and flux ripples significantly. Furthermore, with the adoption of the SVM technique, a constant switching frequency is obtained. However, akin to the conventional DTC, the low-speed performance is still an issue to be resolved.

To achieve sensorless operation of an IPMSM drive at extremely low speeds and at standstill, high-frequency (HF) signal injection offers a reliable solution. However, this method cannot be used at higher speeds, and other forms of observers have to be adopted [8], [13]. Numerous HF signal injection techniques for vector-controlled IPMSM drives [9]–[11], [17], switched reluctance [14], and induction machines [15] have been reported in recent literature. The method proposed by Andreescu *et al.* [17] for hybrid position and speed estimation is seen to be capable of sensorless operation of the IPMSM at very low speeds but with poor dynamic performance. Another hybrid position and speed estimation observer was proposed by

Manuscript received October 2, 2008; revised May 24, 2009 and July 29, 2009; accepted October 12, 2009. Date of publication February 8, 2010; date of current version October 13, 2010.

S. Sayeef is with the University of Wollongong, Wollongong, N.S.W. 2522, Australia (e-mail: saad@uow.edu.au).

G. Foo and M. F. Rahman are with the University of New South Wales, Sydney, N.S.W. 2052, Australia (e-mail: gilbert.foo@student.unsw.edu.au; f.rahman@unsw.edu.au).

Color versions of one or more of the figures in this paper are available online at http://ieeexplore.ieee.org.

Digital Object Identifier 10.1109/TIE.2010.2041730

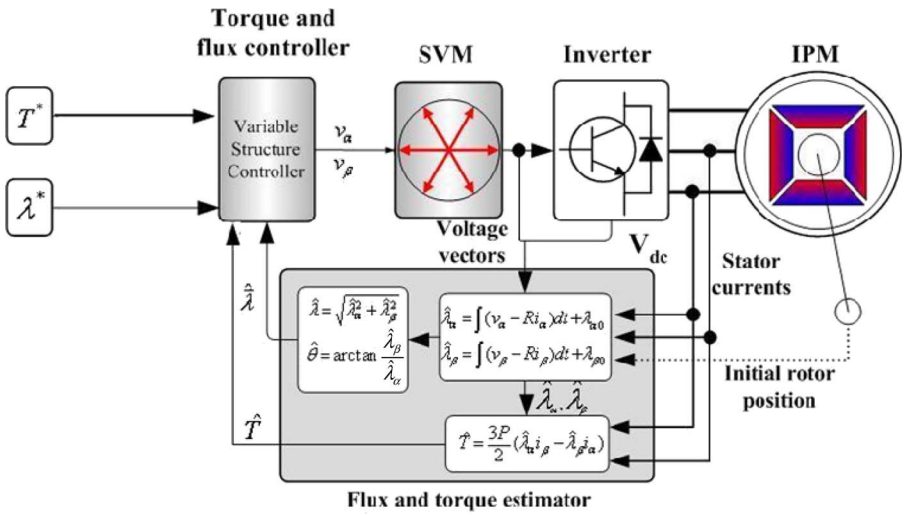

Fig. 1. System diagram of the variable structure direct-torque-controlled IPM drive.

Silva *et al.* [18] which works well for surface permanent magnet synchronous motors but is not applicable to IPMSMs due to their saliency. Similar approaches for direct-torque-controlled IPMSMs are still scarce.

This paper presents a VS-DTC IPMSM drive which is capable of handling zero speed. The drive uses HF signal injection techniques only at low speeds to extract the machine position information. This position information is then used to estimate the flux and torque at low speeds using the current model. Flux and torque estimation at higher speeds is performed using position information obtained from a sliding mode observer. The effects of forward voltage drop and dead time across power devices in a three-phase inverter are compensated for using a lookup table [19], based on the direction of current, to further improve the performance of the drive at low speeds.

The VS-DTC technique and its control law are discussed in the next section, followed by an explanation of the HF signal injection method implemented for low-speed operation. The handover of position extraction methods for flux and torque estimation at low and high speeds is also explained briefly. Experimental results to examine the capability of the proposed HF signal injection algorithm in accurately estimating the rotor position and speed of a VS-DTC drive at very low speeds including standstill are presented.

II. IPM Machine Equations

The equations of an IPM synchronous motor on the $d-q$ rotating coordinates are

$$\begin{bmatrix} v_d \\ v_q \end{bmatrix} = \begin{bmatrix} R + pL_d & -\omega_{\rm re} L_q \\ \omega_{\rm re} L_d & R + pL_q \end{bmatrix} \begin{bmatrix} i_d \\ i_q \end{bmatrix} + \begin{bmatrix} 0 \\ \omega_{\rm re} \lambda_f \end{bmatrix} \quad (1)$$

$$T = \frac{3P\lambda_s}{4L_d L_q} \left[2\lambda_f L_q \sin\delta - \lambda_s (L_q - L_d) \sin 2\delta \right] \quad (2)$$

where

R	stator armature resistance, in ohms;
L_d, L_q	direct and quadrature inductances, respectively, in henries;
$w_{\rm re}$	electrical rotor speed, in radians per second;
T	electromagnetic torque, in newton meters;
P	number of pole pairs;
λ_s, λ_f	stator and rotor flux linkages, respectively;
p	differential operator;
δ	load angle;
v_d, v_q, i_d, i_q	voltages and currents in the rotor reference frame.

III. VSC Scheme

The variable structure control (VSC) scheme is based on the design of a discontinuous control signal that drives the system toward special manifolds in the state space. These switching surfaces are chosen in a way that the system will have the desired behavior as the states converge to the manifolds [7]. A block diagram of the variable structure DTC is shown in Fig. 1. A nonlinear variable structure controller calculates the most appropriate stator voltage vectors to drive the flux and torque to track their references. A speed PI controller in the outer loop (not shown in the figure) produces the reference torque command for the torque controller.

The first step in the VSC design is to design or set a switching surface so that the system state restricted to this surface has desired behaviors such as stability, tracking, or regulation. The second step is to design a switching control law that will drive the state trajectories to the switching surface and retain them on the surface upon interception, which is achieved using a Lyapunov approach.

The control objectives are to track the desired torque and flux trajectories. As explained in [7], the switching surface is set as $S = [\, S_1 \quad S_2 \,]^{\rm T}$

$$S_1 = e_T(t) + K_1 \int_0^t e_T(\tau) d\tau - e_T(0) \quad (3)$$

$$S_2 = e_\lambda(t) + K_2 \int_0^t e_\lambda(\tau) d\tau - e_\lambda(0) \quad (4)$$

where $e_T = T_{\rm ref} - T$ and $e_\lambda = \lambda_{\rm ref} - \lambda$ are the errors between the references and the estimated values of the torque and the square of the flux. K_1 and K_2 are positive control gains. Torque regulation is represented by $S_1 = 0$, and tracking of the square of the flux magnitude is represented by $S_2 = 0$. When the system states reach the sliding manifold and stay on the surface, then $S_1 = S_2 = \dot{S}_1 = \dot{S}_2 = 0$, where $\dot{S}$ is the derivative of S. From (3) and (4), when the derivatives of S are equal to zero, (5) and (6) are obtained

$$\frac{d}{dt}e_T = -K_1 e_T \tag{5}$$

$$\frac{d}{dt}e_\lambda = -K_2 e_\lambda. \tag{6}$$

For the derivatives of the errors (e_T and e_λ) to converge to zero, K_1 and K_2 need to be positive constants and are chosen according to the desired system dynamics as the amplitudes determine the convergence rates of the error dynamics. The design task is then reduced to enforcing sliding mode in the manifolds $S_1 = 0$ and $S_2 = 0$ with discontinuous stator voltage space vectors.

A VSC law is then required to be designed for the state trajectories to be driven to the intersection of the aforementioned switching surfaces and for them to remain on the surfaces for all subsequent time upon interception. To fulfill this requirement, a VSC controller is designed to generate the stator voltage vector for the SVM modulator.

The state equations obtained after transformation of the IPMSM system equation (1) from the $d-q$ coordinate to the $\alpha-\beta$ coordinate are shown in [8], and the resulting torque and flux are given by

$$T = \frac{3P}{2}(\lambda_\alpha i_\beta - \lambda_\beta i_\alpha) \tag{7}$$

$$\lambda = \lambda_\alpha^2 + \lambda_\beta^2 \tag{8}$$

where T is the estimated torque, P is the number of pole pairs, and λ is the square of the stator flux linkage norm.

The motion projection of the system equations on the S subspace is derived by differentiating vector S

$$\dot{S}_1 = \dot{e}_T + K_1 e_T = (\dot{T}_{\rm ref} - \dot{T}) + K_1(T_{\rm ref} - T) \tag{9}$$

$$\dot{S}_2 = \dot{e}_\lambda + K_2 e_\lambda = K_2(\lambda_{\rm ref} - \lambda) + (\dot{\lambda}_{\rm ref} - \dot{\lambda}). \tag{10}$$

Substituting for T, λ, and their derivatives using (7) and (8) results in

$$\dot{\underline{S}} = \underline{F} + \underline{D} \cdot \underline{u} \tag{11}$$

where $\underline{u} = [\, v_\alpha \quad v_\beta \,]^{\rm T}$ is the control input and

$$\underline{D} = \begin{bmatrix} -\frac{3}{2}P\left(i_\beta - \frac{\lambda_\beta}{L_d}\right) & -\frac{3}{2}P\left(\frac{\lambda_\alpha}{L_d} - i_\alpha\right) \\ -2\lambda_\alpha & -2\lambda_\beta \end{bmatrix} \tag{12}$$

$$\begin{aligned} F_1 = &-\frac{3}{2}P\left(\lambda_\alpha\left(\omega_{\rm re}(L_d - L_q)/L_d \cdot i_\alpha - \frac{R}{L_d}i_\beta - \frac{1}{L_d}e_\beta\right)\right. \\ &\left. -\lambda_\beta\left(-\frac{R}{L_d}i_\alpha - \omega_{\rm re}(L_d - L_q)/L_d \cdot i_\beta - \frac{1}{L_d}e_\alpha\right)\right) \\ &+ K_1 e_T \\ F_2 = &\, K_2 e_\lambda + 2\lambda_\alpha R i_\alpha + 2\lambda_\beta R i_\beta \end{aligned} \tag{13}$$

where e_α and e_β are the salient electromotive forces (EMFs) described in Section VI. By setting $\underline{u}$ as that in (14), (11) can be rewritten as (15)

$$\underline{u} = -\underline{D}^{-1}[\underline{F} + K\,{\rm sgn}(s)] \tag{14}$$

$$\dot{\underline{S}} = \underline{F} + \underline{D}\underline{u} = -K\,{\rm sgn}(s) \tag{15}$$

where $K = \begin{bmatrix} \mu_1 & 0 \\ 0 & \mu_2 \end{bmatrix}$ and μ_1 and μ_2 are constant positive control gains. Larger values of μ_1 and μ_2 increase the robustness of the drive. The control law in [7] requires gain scheduling, and no guidelines in the control gain selection were provided in [7]. It has been confirmed in our experiments that the adoption of constant gains for the control law in [7] leads to system instability. Since the control gains proposed in (14) are not speed dependent, it requires no gain scheduling and is therefore superior to the scheme proposed in [7].

The stator voltage vectors in the VSC strategy are adaptive to error amplitudes. The VSC scheme also allows more voltage vectors to be applied during each sampling interval, which is divided into more subintervals, thereby increasing the control resolution and significantly reducing torque and flux ripples. This control scheme produces better results for transient, steady-state, and dynamic operations due to better control resolution.

IV. HF Signal Injection

Several HF signal injection methods can be found in the literature. These methods can be classified into $\alpha-\beta$ frame rotating injection [9], $d-q$ frame pulsating injection [10], and $d-q$ frame rotating injection [11]. In this paper, the $d-q$ frame persistent HF rotating carrier injection is implemented, where an alternating voltage is used for injection. A carrier excitation signal fluctuating at angular frequency ω_c and having amplitude V_c, as shown in (16), is superimposed on the d component of the stator voltage in the estimated rotor reference frame [10]

$$\begin{bmatrix} v_{dc} \\ v_{qc} \end{bmatrix} = V_c \cos(\omega_c t)\begin{bmatrix} 1 \\ 0 \end{bmatrix}. \tag{16}$$

The frequency of the injected voltage carrier ω_c should be high enough to ensure sufficient spectral separation between itself and the fundamental excitation to reduce the requirements of the bandpass filters.

An alternating HF current response is detected in the q-direction of the estimated rotor reference frame with its

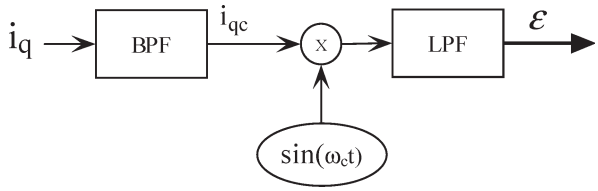

Fig. 2. Demodulation scheme used to obtain the position error signal.

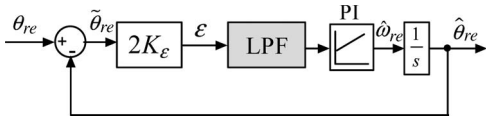

Fig. 3. PLL.

amplitude modulated by the rotor position estimation error, as shown in (17). The method of the demodulation process is shown in Fig. 2. The HF component of the measured current in the q-direction i_{qc} is separated from the fundamental component by bandpass filtering of the q component of the measured current. The HF current signal is then demodulated and low-pass filtered (LPF) to extract an error signal given by (18)

$$i_{\hat{q}c} = \frac{V_c}{\omega_c}\frac{L_q - L_d}{2L_dL_q}\cos(\omega_c t)\sin\left[2(\theta_{\rm re} - \hat{\theta}_{\rm re})\right] \tag{17}$$

$$\varepsilon = LPF\left\{i_{qc}\sin(\omega_c t)\right\}. \tag{18}$$

This error signal is ideally [10]

$$\varepsilon = K_\varepsilon \sin(2\tilde{\theta}_{\rm re}) \tag{19}$$

where $K_\varepsilon = (V_c/\omega_c)((L_q - L_d)/4L_dL_q)$ and $\tilde{\theta}_{\rm re} = \theta_{\rm re} - \hat{\theta}_{\rm re}$ is the estimated error of the rotor position. Assuming that the estimated error is small, (19) can be approximated by

$$\varepsilon \approx 2K_\varepsilon \tilde{\theta}_{\rm re}. \tag{20}$$

Instead of using a bandpass filter to obtain the HF component of i_q, the algorithm shown in (21) is used. This algorithm can be interpreted as a high-pass filter and is chosen due to its lower computational cost than relevant bandpass filters

$$i_{qc} = i_q - \frac{1}{T_c}\sum_{n=0}^{n=k} i_{q_n}\cdot\Delta T \tag{21}$$

where $T_c = 2\pi/\omega_c$ is the period of the HF carrier signal, ΔT is the sampling period, and $k = (T_c/\Delta T) - 1$.

The low-pass filtering, shown in Fig. 3, is implemented using two filters, namely, a moving-average filter and a first-order low-pass filter. The moving-average filter eliminates the angular frequency ω_c and its multiples effectively with only a short time delay, while the first-order low-pass filter reduces stochastic noise more effectively than the moving-average filter.

A PI controller cascaded with an integrator is then used to drive the error signal to zero and to obtain the estimated rotor position signal. Hence, the closed-loop system constitutes a phase-locked loop (PLL), as shown in Fig. 3.

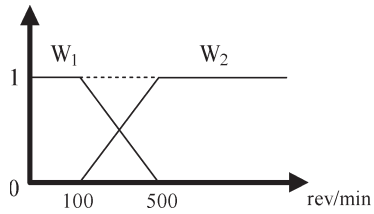

Fig. 4. Weighting coefficients for changeover of algorithms.

The estimated rotor position information is then used for estimating the stator flux linkages and torque using the current model of the IPM machine, as shown in

$$\lambda_d = L_d i_d + \lambda_f$$

$$\lambda_q =; L_q i_q \tag{22}$$

$$T_e = \frac{3}{2}P(\lambda_d i_q - \lambda_q i_d). \tag{23}$$

V. Changeover Algorithm

The HF signal injection method to obtain information of rotor position becomes difficult to apply at high speeds mainly because the alternating exciting frequency must be completely off a fundamental wave frequency as a prerequisite. The rotor position information from a sliding observer is used at high speeds, as outlined in the next section. The change of algorithms at low and high speeds has been realized by using weight coefficients W_1 and W_2 to determine the input to the flux controller [20]. In this case, W_1 represents the weighting for rotor position information obtained during HF signal injection, while W_2 is the weighting of rotor position obtained from the sliding observer. This is shown in Fig. 4, where W_1 fully dominates below 100 r/min and W_2 above 500 r/min. The crossover of algorithms does not affect the estimated position as $W_1 + W_2 = 1$.

VI. Adaptive Sliding Observer

The IPM machine model in (1) can be transformed to the stationary $\alpha-\beta$ reference frame by rewriting the impedance matrix in (1) symmetrically before $d-q$ to $\alpha-\beta$ coordinate transformation to obtain

$$\begin{bmatrix} v_\alpha \\ v_\beta \end{bmatrix} = \begin{bmatrix} R + pL_d & \omega_{\rm re}(L_d - L_q) \\ -\omega_{\rm re}(L_d - L_q) & R + pL_d \end{bmatrix}\begin{bmatrix} i_\alpha \\ i_\beta \end{bmatrix} + \left\{(L_d - L_q)(\omega_{\rm re} i_d - \dot{i}_q) + \omega_{\rm re}\lambda_f\right\}\begin{bmatrix} -\sin\theta_{\rm re} \\ \cos\theta_{\rm re} \end{bmatrix}. \tag{24}$$

The right-hand term in (24) is defined as the EMF due to saliency and rewritten into

$$e = \begin{bmatrix} e_\alpha \\ e_\beta \end{bmatrix} = \left\{(L_d - L_q)(\omega_{\rm re} i_d - \dot{i}_q) + \omega_{\rm re}\lambda_f\right\}\begin{bmatrix} -\sin\theta_{\rm re} \\ \cos\theta_{\rm re} \end{bmatrix}. \tag{25}$$

Using the salient EMF model in (24), a current model of IPM synchronous motors can be described by

$$\begin{bmatrix}\dot{i}_\alpha\\ \dot{i}_\beta\end{bmatrix}=\begin{bmatrix}-R/L_d & -\omega_{\rm re}(L_d-L_q)/L_d\\ \omega_{\rm re}(L_d-L_q)/L_d & -R/L_d\end{bmatrix}\begin{bmatrix}i_\alpha\\ i_\beta\end{bmatrix}+\begin{bmatrix}-1/L_d & ;0\\ 0 & -1/L_d\end{bmatrix}\begin{bmatrix}e_\alpha\\ e_\beta\end{bmatrix}+1/L_d\begin{bmatrix}v_\alpha\\ v_\beta\end{bmatrix}. \quad (26)$$

An adaptive flux observer is designed based on the stator current model (26) and is expressed as

$$\begin{bmatrix}\dot{\hat{i}}\\ \dot{\hat{e}}\end{bmatrix}=\begin{bmatrix}\hat{A}_{11} & A_{12}\\ 0 & \hat{A}_{22}\end{bmatrix}\cdot\begin{bmatrix}i\\ \hat{e}\end{bmatrix}+\begin{bmatrix}B_1\\ 0\end{bmatrix}v+K\,\mathrm{sgn}(s) \quad (27)$$

where

$$\hat{i}=[\,\hat{i}_\alpha\quad\hat{i}_\beta\,]^{\rm T}\qquad\hat{e}=[\,\hat{e}_\alpha\quad\hat{e}_\beta\,]^{\rm T}\qquad s=\begin{bmatrix}i_\alpha-\hat{i}_\alpha\\ i_\beta-\hat{i}_\beta\end{bmatrix}$$

$$\hat{A}_{11}=-(R/L_d)\cdot I+\hat{\omega}_{\rm re}(L_d-L_q)/L_d\cdot J$$

$$\hat{A}_{22}=\hat{\omega}_{\rm re}J$$

$$K=\begin{bmatrix}d1 & 0\\ 0 & d2\\ -d1\cdot L_d\cdot q1 & \hat{\omega}_{\rm re}\cdot d2\cdot L_d\\ -d1\cdot L_d\cdot\hat{\omega}_{\rm re} & -d2\cdot L_d\cdot q2\end{bmatrix}$$

where $d1$, $d2$, $q1$, and $q2$ are positive observer gains that are determined by Lyapunov stability analysis. The error dynamics for the current estimation is given in (28), where $\bar{i}_\alpha=i_\alpha-\hat{i}_\alpha$, $\bar{i}_\beta=i_\beta-\hat{i}_\beta$, $\bar{e}_\alpha=e_\alpha-\hat{e}_\alpha$, and $\bar{e}_\beta=e_\beta-\hat{e}_\beta$ are the differences between the estimated and measured currents and back EMFs. $d1$ and $d2$ are positive observer gains

$$\begin{aligned}\dot{\bar{i}}_\alpha=&-1/L_d\cdot\bar{e}_\alpha-d1\cdot\mathrm{sgn}(i_\alpha-\hat{i}_\alpha)\\ &-(\omega_{\rm re}-\hat{\omega}_{\rm re})\cdot(1-L_q/L_d)\cdot i_\beta\\ \dot{\bar{i}}_\beta=&-1/L_d\cdot\bar{e}_\beta-d2\cdot\mathrm{sgn}(i_\beta-\hat{i}_\beta)\\ &+(\omega_{\rm re}-\hat{\omega}_{\rm re})\cdot(1-L_q/L_d)\cdot i_\alpha.\end{aligned} \quad (28)$$

To prove the convergence of the aforementioned observer, the Lyapunov candidate function is chosen as

$$V=\frac{1}{2}\left(\bar{i}_\alpha^2+\bar{i}_\beta^2\right). \quad (29)$$

The time derivative of Lyapunov function $\dot{V}$ is

$$\begin{aligned}\dot{V}=&\,\bar{i}_\alpha\cdot\dot{\bar{i}}_\alpha+\bar{i}_\beta\cdot\dot{\bar{i}}_\beta\\ =&-\bar{i}_\alpha\cdot(\bar{e}_\alpha/L_d+(\omega_{\rm re}-\hat{\omega}_{\rm re})\cdot(1-L_q/L_d)\cdot i_\beta)\\ &-\bar{i}_\beta\cdot(\bar{e}_\beta/L_d-(\omega_{\rm re}-\hat{\omega}_{\rm re})\cdot(1-L_q/L_d)\cdot i_\alpha)\\ &-d1\cdot|\bar{i}_\alpha|-d2\cdot|\bar{i}_\beta|.\end{aligned} \quad (30)$$

$d1$ and $d2$ have to be large enough to ensure robustness of the observer to disturbance, parameter mismatches, and speed estimation error. At least, if $d1>|\bar{e}_\alpha/L_d+(\omega_{\rm re}-\hat{\omega}_{\rm re})\cdot(1-L_q/L_d)\cdot i_\beta|$ and $d2>|\bar{e}_\beta/L_d-(\omega_{\rm re}-\hat{\omega}_{\rm re})\cdot(1-L_q/L_d)\cdot i_\alpha|$, V decays to zero; then, $\bar{i}_\alpha$ and $\bar{i}_\beta$ are equal to zero, resulting in the estimated currents converging to their values. After sliding mode motion occurs, the equivalent control information of the two discontinuous high switching control components is extracted in

$$\begin{aligned}\bar{e}_\alpha=&-d1\cdot L_d\cdot\mathrm{sgn}(i_\alpha-\hat{i}_\alpha)\\ \bar{e}_\beta=&-d2\cdot L_d\cdot\mathrm{sgn}(i_\beta-\hat{i}_\beta)\\ \dot{\bar{e}}_\alpha=&-\bar{e}_\beta\hat{\omega}_{\rm re}+d1\cdot L_d\cdot q1\cdot\mathrm{sgn}(i_\alpha-\hat{i}_\alpha)\\ &-\hat{\omega}_{\rm re}\cdot d2\cdot L_d\cdot\mathrm{sgn}(i_\beta-\hat{i}_\beta)\\ =&-\bar{e}_\beta\hat{\omega}_{\rm re}-q1\cdot\bar{e}_\alpha+\bar{e}_\beta\hat{\omega}_{\rm re}\\ =&-q1\cdot\bar{e}_\alpha\end{aligned} \quad (31)$$

$$\begin{aligned}\dot{\bar{e}}_\beta=&\,\bar{e}_\alpha\hat{\omega}_{\rm re}+d1\cdot L_d\cdot\hat{\omega}_{\rm re}\cdot\mathrm{sgn}(i_\alpha-\hat{i}_\alpha)\\ &+d2\cdot L_d\cdot q2\cdot\mathrm{sgn}(i_\beta-\hat{i}_\beta)\\ =&\,\bar{e}_\alpha\hat{\omega}_{\rm re}-\bar{e}_\alpha\hat{\omega}_{\rm re}-q2\cdot\bar{e}_\beta\\ =&-q2\cdot\bar{e}_\beta.\end{aligned} \quad (32)$$

Equation (32) ensures that the errors ($\bar{e}_\alpha$ and $\bar{e}_\beta$) converge to zero if $q1$ and $q2$ are positive gains and chosen for the desired system dynamics. The convergence rates of the error dynamics are determined by $q1$ and $q2$.

The EMF due to saliency in (25) contains rotor spatial information that can be retrieved for position estimation. At zero speed, the EMF is nonzero only if $\dot{i}_q\neq 0$. The rotor position is retrieved using the phase angles of $\hat{e}_\alpha$ and $\hat{e}_\beta$ as shown in

$$\hat{\theta}_{\rm re}=\tan^{-1}(-\hat{e}_\alpha/\hat{e}_\beta). \quad (33)$$

The estimated stator flux vector is then obtained using the IPM motor current model.

VII. Rotor Speed Estimation

A simplified Kalman filter was developed to minimize the time delay or lag of the estimated speed behind the actual rotor speed and to improve the accuracy of speed estimation during transients. This method was originally used for speed estimation from sine/cosine resolver signals [12]. The Kalman filter is adopted in this paper to estimate speed using rotor position information extracted from the HF signal injection algorithm at very low speeds and from the observed salient EMF at higher speeds.

A state-space model for the rotor position $\theta_{\rm re}(k)$ and speed $\omega_{\rm re}(k)$ [12] is shown in

$$\begin{aligned}\theta_{\rm re}(k+1)=&\,\theta_{\rm re}(k)+T\cdot\omega_{\rm re}(k)\\ \omega_{\rm re}(k+1)=&\,\omega_{\rm re}(k)+w'(k)\\ w'(k+1)=&\,w'(k)+w(k)\end{aligned} \quad (34)$$

where T is the sampling period and $w(k)$ is white noise of zero mean. The speed is predicted as a ramp change and hence should be modeled as a double integration of the noise $w(k)$ to avoid a lagging estimate during transients.

$\hat{e}_\alpha$ and $\hat{e}_\beta$ from (27) contain sine and cosine components of the rotor position and can be nominalized as

$$\begin{bmatrix}y_1\\ y_2\end{bmatrix}=\begin{bmatrix}\cos\theta_{\rm re}(k)\\ \sin\theta_{\rm re}(k)\end{bmatrix}+\begin{bmatrix}v_1(k)\\ v_2(k)\end{bmatrix}. \quad (35)$$

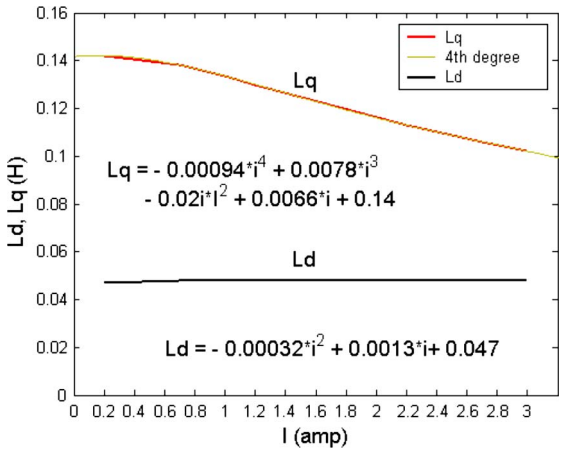

Fig. 5. Measured and interpolated d- and q-axis inductances as a function of the operating current.

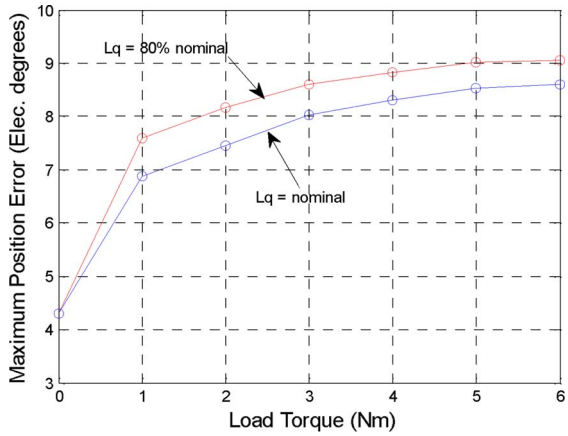

Fig. 6. Maximum position estimation error versus load torque for nominal L_q and 80% nominal L_q.

A state-space model is built with state vector $x = [\theta \quad \omega_r \quad w']^{\mathrm{T}}$

$$\begin{aligned} x(k+1) &= Fx(k) + w(k) \\ y(k) &= h\left(x(k)\right) + v(k) \end{aligned} \tag{36}$$

where $F = \begin{bmatrix} 1 & T & 0 \\ 0 & 1 & 1 \\ 0 & 0 & 1 \end{bmatrix}$ and $h(x) = \begin{bmatrix} \cos(\theta_{\mathrm{re}}) \\ \sin(\theta_{\mathrm{re}}) \end{bmatrix}$. The Kalman filter gain is expressed as

$$K = \begin{bmatrix} 0 & k_1 \\ 0 & k_2 \\ 0 & k_3 \end{bmatrix} \cdot \begin{bmatrix} \cos\hat{\theta}_{\mathrm{re}} & \sin\hat{\theta}_{\mathrm{re}} \\ -\sin\hat{\theta}_{\mathrm{re}} & \cos\hat{\theta}_{\mathrm{re}} \end{bmatrix}. \tag{37}$$

The gains can be precalculated in the filter design procedures using MATLAB's *dlqe* command. The final equations [12] of the rotor position and speed are written explicitly as

$$\begin{aligned} \varepsilon(k) &= y_2(k)\cos\hat{\theta}_{\mathrm{re}}(k) - y_1\sin\hat{\theta}_{\mathrm{re}}(k) \\ \hat{\theta}_{\mathrm{re}}(k+1) &= \hat{\theta}_{\mathrm{re}}(k) + T\hat{\omega}_{\mathrm{re}}(k) + k_1\varepsilon(k) \\ \hat{\omega}_{\mathrm{re}}(k+1) &= \hat{\omega}_{\mathrm{re}}(k) + w'(k) + k_2\varepsilon(k) \\ w'(k+1) &= w'(k) + k_3\varepsilon(k). \end{aligned} \tag{38}$$

The simplified Kalman filter was used for speed estimation of the sensorless VS-DTC IPM drive from standstill up to a rated speed.

VIII. Parameter Sensitivity Analysis

The HF signal injection algorithm proposed in Section IV to obtain rotor position information at very low speeds including standstill is parameter independent and therefore is not affected by any variation of machine parameters. However, flux estimation using the current model of the IPM machine involves the parameters L_d and L_q. The accuracy of the flux observation is critical for the robustness of the proposed drive system. Therefore, it is necessary to investigate the variations of the d- and q-axis inductances for different operating conditions.

Iron saturation reduces air gap flux density, causing IPM machines to demonstrate inductances that vary as a function of the operating point. Fig. 5 shows the measured and interpolated d- and q-axis inductances from the experimental machine. For this motor, the q-axis inductance is about 2.3 times greater than the d-axis inductance. Both inductances vary as a function of the operating current. The functions can be presented by polynomials, as shown in Fig. 5. It is seen that L_d does not vary much within the operating range and can therefore be considered constant. On the contrary, the value of L_q decreases with increasing operating current.

The effects of L_q detuning on the position estimation error have been investigated. Since the flux observer requires the values of L_d and L_q at low speeds, experimental results were undertaken when the machine was operated with various loads up to full (rated) load at various speeds. Fig. 6 shows a plot showing the peak position estimation errors for various load torques for nominal L_q and 80% nominal L_q. The HF signal injection observer produces a larger error with the increase of load and L_q detuning. Similar observations were made at other speeds.

IX. Experimental Results

The performance of the proposed sensorless VS-DTC scheme with HF signal injection was tested experimentally. A block diagram of the sensorless VS-DTC drive can be seen in Fig. 7. The lower part of Fig. 7 includes the PLL indicated by (18) and (19). A DS1104 DSP card was used to carry out the real-time algorithm. A three-phase insulated-gate bipolar transistor intelligent power module is used for an inverter.

Coding of real-time control software was done using C language. The PWM signals were generated on a DS1104 board. A dc machine whose armature current is separately regulated is used to emulate the load. The parameters of the IPM machine used are shown in Table I.

An incremental encoder was used to obtain the position signal which was solely used for comparison and not for control purposes. The sampling period of the DTC was set to 200 μs. The chosen values of the observer gains $d1$, $d2$, $q1$, and $q2$ are 0.1, 0.1, 1.0, and 1.2, respectively.

Fig. 8 shows the performance of the VS-DTC IPM drive at zero speed, where full load is applied at $t = 0.92$ s and subsequently removed at $t = 3.43$ s. The subplots in Fig. 8 (top to bottom) show the estimated speed, the actual speed obtained from the incremental encoder, the estimated torque, the estimated flux, the speed estimation error, and the rotor position

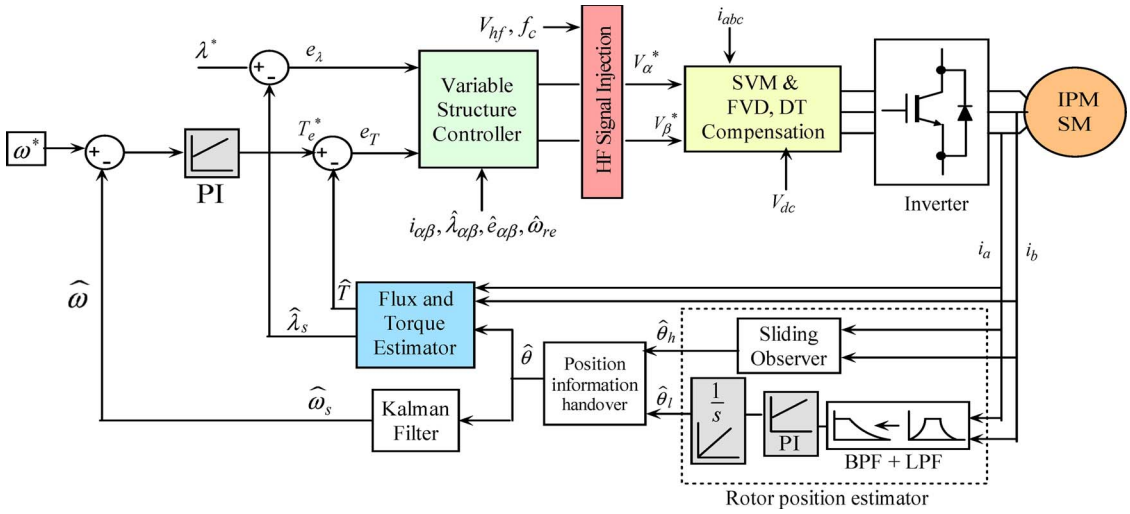

Fig. 7. Block diagram of the sensorless VS-DTC with HF signal injection and a sliding observer.

TABLE I
PARAMETERS OF THE IPMSM USED IN THIS PAPER

Number of pole pairs	P	2
Stator resistance	R	5.8 Ω
Magnet flux linkage	λ_f	0.533 Wb
d-axis inductance	L_d	0.0448 H
q-axis inductance	L_q	0.1024 H
Phase voltage	V	132 V
Phase current	I	3 A
Base speed	w_b	1260 rpm
Rated torque	T_b	6 Nm

estimation error. It can be seen that the estimated speed tracks the actual speed very well with an average mechanical speed estimation error of 0.21 r/min. An increase in the amplitude of the ripples due to the injection of an HF signal is seen in the estimated quantities when full load is applied. The bottom subplot in Fig. 8 shows the position (electrical) estimation error, where the average estimation error is 1.61° (0.028 rad).

The response of the speed, torque, and flux of the fully loaded DTC IPM drive when the speed reference is changed from 10 to −10 r/min is shown in Fig. 9. A smooth transition from positive to negative speed with full load is seen with a very small average mechanical speed estimation error of 0.24 r/min. The average position (electrical) estimation error during the full-load speed reversal is 5.73° (0.1 rad), indicating the accuracy at which the estimated rotor position tracks the actual position.

Fig. 10 shows the estimated and actual speeds, torque, flux, speed estimation error, and position estimation error during a speed reference step change from 5 to −5 r/min and vice versa. The speed reversal in both directions is smooth with insignificant impact on the torque and flux. The average speed estimation error for this case was calculated to be 0.031 r/min. The average position (electrical) estimation error was measured to be 1.4° (0.025 rad).

The extremely low speed performance of the sensorless SVM DTC drive at 5 r/min under full-load condition is shown in Fig. 11. The estimated speed follows the actual speed very well

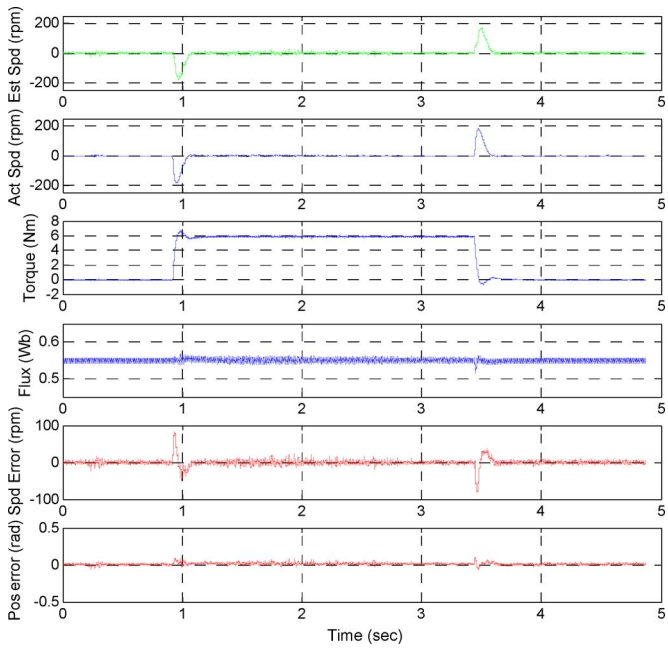

Fig. 8. Speed (estimated and actual), torque, flux, and speed and position estimation error during application and removal of full load at zero speed.

with an average speed estimation error of just 0.055 r/min. The average rotor position (electrical) estimation error was 4.31° (0.075 rad). The results shown in Figs. 8–11 prove the capability of the proposed HF signal injection algorithm in accurately determining the rotor position and speed at very low speeds without a speed sensor during both transient and steady-state operations.

The performance of the changeover algorithm, in handing over the rotor position information between the two observers at low and high speeds, has been investigated and is shown in Fig. 12. It can be seen that the handover of position information from HF signal injection to that from a sliding mode observer takes place smoothly without any glitches. The proposed hand-over algorithm is thus superior to that in [17]. The green lines in both the speed and position subplots indicate the estimated quantities, while the blue lines indicate the actual speed and

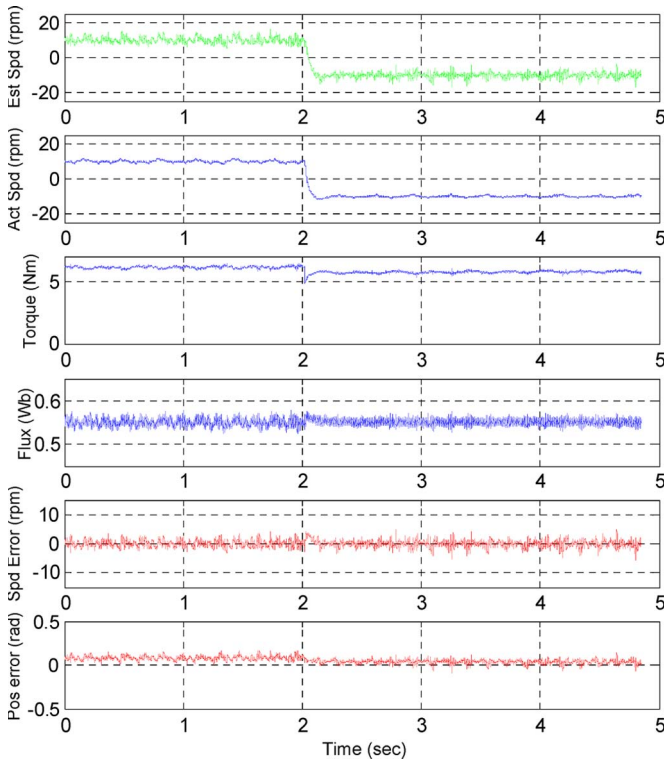

Fig. 9. Speed (estimated and actual), torque, flux, and speed and position estimation error during speed reversal from 10 to −10 r/min with full load.

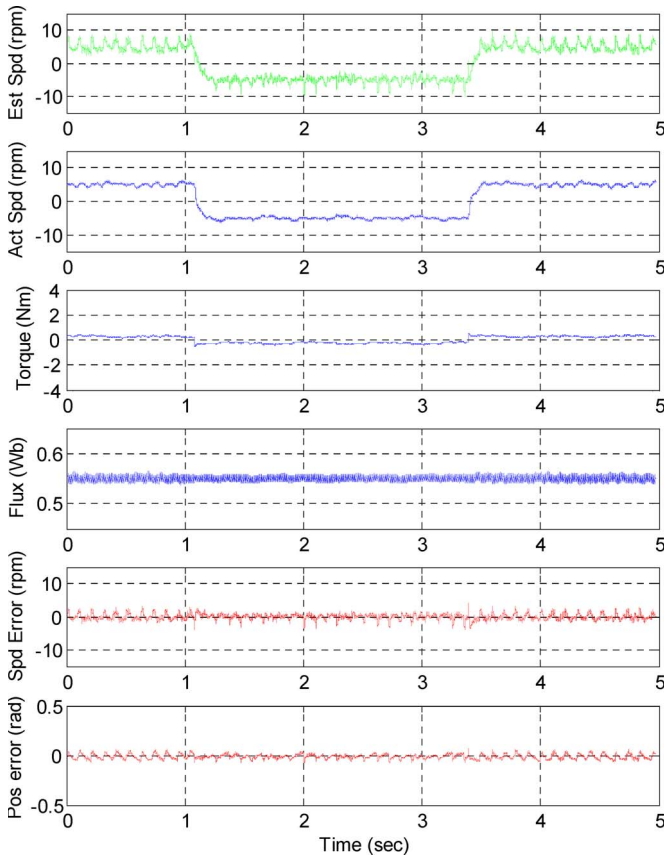

Fig. 10. Speed (estimated and actual), torque, flux, and speed and position estimation error during speed reversal from 5 to −5 r/min and vice versa (unloaded).

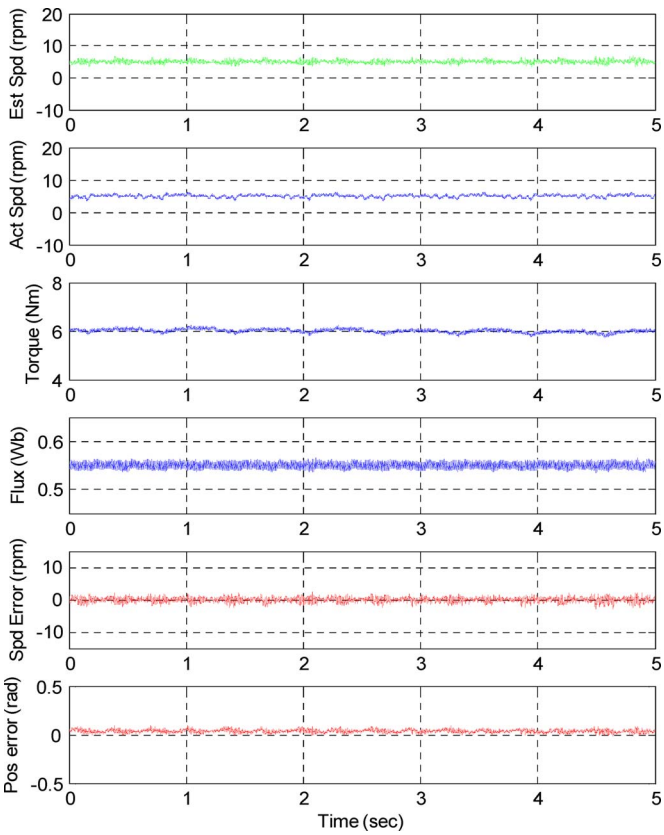

Fig. 11. Speed (estimated and actual), torque, flux, and speed and position estimation error of the sensorless IPM drive at 5 r/min with full load.

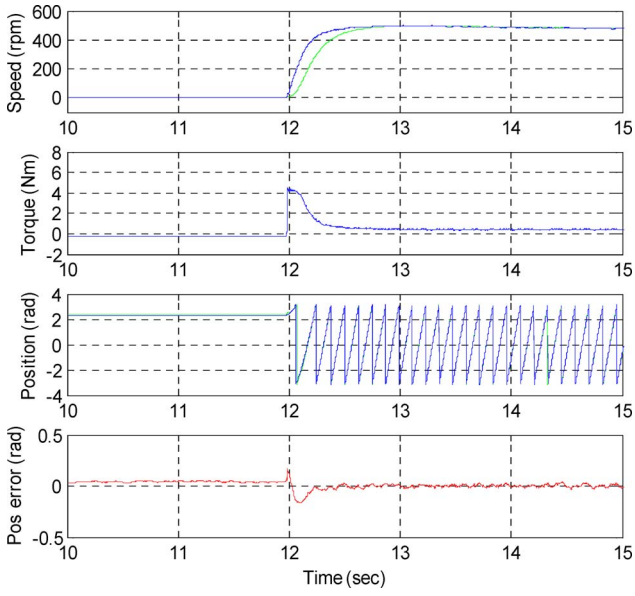

Fig. 12. Dynamic performance—Speed step from 0 to 500 r/min.

position obtained from the encoder. The bottom subplot shows the position estimation error, the average of which was measured to be 1.76° (electrical).

X. Conclusion

The performance of the VS-DTC IPM drive without any speed sensor at low speeds including standstill has been

investigated in this paper. HF signal injection is used to extract the rotor position information at very low speeds below 100 r/min, while a sliding mode observer is used to obtain the position information at speeds greater than 500 r/min. The handover between these two methods is performed using a weighting algorithm which takes place when the drive is operating between 100 and 500 r/min. Results show that the proposed sensorless VS-DTC IPM drive system is able to estimate the rotor position and speed accurately at very low speeds including standstill during both steady-state and dynamic operations under both loaded and unloaded conditions.

The handover of the rotor position information from HF signal injection to that from a sliding mode observer is also seen to take place smoothly without any problems.

It can therefore be concluded that the sensorless operation of the DTC IPM drive from zero to base speed is achieved using the proposed HF signal injection and sliding mode observers.

REFERENCES

[1] M. Depenbrock, "Direct self-control of inverter-fed machine," *IEEE Trans. Power Electron.*, vol. 3, no. 4, pp. 420–429, Oct. 1988.

[2] I. Takahashi and T. Naguchi, "A new quick-response and high-efficiency control strategy of an induction motor," *IEEE Trans. Ind. Appl.*, vol. IA-22, no. 5, pp. 820–827, Sep./Oct. 1986.

[3] C. French and P. Acarnley, "Direct torque control of permanent magnet drives," *IEEE Trans. Ind. Appl.*, vol. 32, no. 5, pp. 1080–1088, Sep./Oct. 1996.

[4] L. Zhong, M. F. Rahman, W. Y. Hu, and K. W. Lim, "Analysis of direct torque control in permanent magnet synchronous motor drives," *IEEE Trans. Power Electron.*, vol. 12, no. 3, pp. 528–536, May 1997.

[5] L. Tang, L. Zhong, M. F. Rahman, and Y. Hu, "A novel direct torque controlled interior permanent magnet synchronous machine drive with low ripple in flux and torque and fixed switching frequency," *IEEE Trans. Power Electron.*, vol. 19, no. 2, pp. 346–354, Mar. 2004.

[6] C. A. Martins, X. Roboam, T. A. Meynard, and A. S. Carvalho, "Switching frequency imposition and ripple reduction in DTC drives by using a multilevel converter," *IEEE Trans. Power Electron.*, vol. 17, no. 2, pp. 286–297, Mar. 2002.

[7] Z. Xu and M. F. Rahman, "Direct torque and flux regulation of an IPM synchronous motor drive using variable control approach," *IEEE Trans. Power Electron.*, vol. 22, no. 6, pp. 2487–2498, Nov. 2007.

[8] M. Barut, S. Bogosyan, and M. Gokasan, "Experimental evaluation of braided EKF for sensorless control of induction motors," *IEEE Trans. Ind. Electron.*, vol. 55, no. 2, pp. 620–632, Feb. 2008.

[9] C. Spiteri, J. Cilia, B. Michallef, and M. Apap, "Sensorless vector control of surface mount PMSM using high frequency injection," in *Proc. Power Electron. Mach. Drives (Conf. Publ. No. 487)*, Apr. 16–18, 2002, pp. 44–48.

[10] M. Corley and R. D. Lorenz, "Rotor position and velocity estimation for a salient-pole permanent magnet synchronous machine at standstill and high speeds," *IEEE Trans. Ind. Appl.*, vol. 43, no. 4, pp. 784–789, Jul./Aug. 1998.

[11] C. Caruana, G. M. Asher, K. J. Bradley, and M. S. Woolfson, "Flux position estimation in cage induction machines using synchronous injection and Kalman filtering," *IEEE Trans. Ind. Appl.*, vol. 39, no. 5, pp. 1372–1378, Sep./Oct. 2003.

[12] L. Harnefors, "Speed estimation from noisy resolver signals," in *Proc. 6th Int. Conf. Power Electron. Variable Speed Drives (Conf. Publ. No. 429)*, Sep. 23–25, 1996, pp. 279–282.

[13] Z. Xu and M. F. Rahman, "An adaptive sliding stator flux observer for a direct-torque-controlled IPM synchronous motor drive," *IEEE Trans. Ind. Electron.*, vol. 54, no. 5, pp. 2398–2406, Oct. 2007.

[14] A. Khalil, S. Underwood, I. Hussain, H. Klode, B. Lequesne, S. Gopalakrishnan, and A. M. Omekanda, "Four-quadrant pulse injection and sliding-mode-observer-based sensorless operation of a switched reluctance machine over entire speed range including zero speed," *IEEE Trans. Ind. Electron.*, vol. 43, no. 3, pp. 714–723, May/Jun. 2007.

[15] Q. Gao, G. Asher, and M. Sumner, "Sensorless position and speed control of induction motors using high-frequency injection and without offline precommissioning," *IEEE Trans. Ind. Electron.*, vol. 54, no. 5, pp. 2474–2481, Oct. 2007.

[16] B. Nahid-Mobarakeh, F. Meibody-Tabar, and F.-M. Sargos, "Back EMF estimation-based sensorless control of PMSM: Robustness with respect to measurement errors and inverter irregularities," *IEEE Trans. Ind. Electron.*, vol. 43, no. 2, pp. 485–494, Mar./Apr. 2007.

[17] G.-D. Andreescu, C. I. Pitic, F. Blaabjerg, and I. Boldea, "Combined flux observer with signal injection enhancement for wide speed-range sensorless direct torque control of IPMSM drives," *IEEE Trans. Energy Convers.*, vol. 23, no. 2, pp. 393–402, Jun. 2008.

[18] C. Silva, G. M. Asher, and M. Sumner, "Hybrid rotor position observer for wide-speed sensorless PM motor drives including zero speed," *IEEE Trans. Ind. Electron.*, vol. 53, no. 2, pp. 373–378, Apr. 2006.

[19] S. Sayeef and M. F. Rahman, "Improved low speed performance of a PI-DTC interior PM machine with compensations of dead-time effects and forward voltage drops," in *Proc. Int. Conf. Power Electron.*, Oct. 22–26, 2007, pp. 906–911.

[20] G. Foo, S. Sayeef, and M. F. Rahman, "Sensorless direct torque and flux control of an IPM synchronous motor drive at low speed and standstill," in *Proc. Conf. Rec. EPE-PEMC*, Sep. 1–3, 2008, pp. 2269–2274.

[21] R. Morales-Caporal and M. Pacas, "Encoderless predictive direct torque control for synchronous reluctance machines at very low and zero speed," *IEEE Trans. Ind. Electron.*, vol. 55, no. 12, pp. 4408–4416, Dec. 2008.

[22] T. Geyer, G. Papafotiou, and M. Morari, "Model predictive direct torque control—Part I: Concept, algorithm, and analysis," *IEEE Trans. Ind. Electron.*, vol. 56, no. 6, pp. 1894–1905, Jun. 2009.

Saad Sayeef (S'03–M'08) received the B.E. degree (first-class honor) in electrical and electronics engineering from The University of Auckland, Auckland City, New Zealand, in 2002 and the Ph.D. degree from the University of New South Wales, Sydney, Australia, in 2009.

He was an Electronics Design Engineer with Fisher and Paykel Appliances, Ltd., Auckland City, until 2004. Since 2009, he has been a Postdoctoral Research Fellow with the University of Wollongong, Wollongong, Australia. His research interests include power electronics, motor drive systems, and renewable energy technologies.

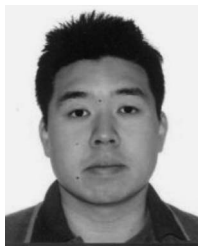

Gilbert Foo (S'06) received the Diploma in electrical and electronics engineering from INTI College, Subang Jaya, Malaysia, in 2004 and the B.E. degree (first-class honor) from the University of New South Wales, Sydney, Australia, in 2007, where he is currently working toward the Ph.D. degree.

His research interests are in electrical machines and drives.

Mr. Foo is a member of the IEEE Industrial Electronics Society, the IEEE Power Electronics Society, and the IEEE Industry Applications Society.

M. F. Rahman (M'79–SM'96) received the B.E. degree (first-class honor) from Bangladesh University of Engineering and Technology, Dhaka, Bangladesh, in 1972 and the M.E. and Ph.D. degrees from the University of Manchester Institute of Science and Technology, Manchester, U.K., in 1975 and 1978, respectively.

He was a System Design Engineer with the General Electric Company, U.K., and with Rugby for two years. In 1980, he joined the National University of Singapore, Singapore. In 1988, he joined the University of New South Wales, Sydney, Australia, as a Senior Lecturer, where he is currently a Full Professor. His research interests are in electrical machines, drives, and power electronics.

Dr. Rahman is a member of the IEEE Industrial Electronics Society, the IEEE Power Electronics Society, and the IEEE Industry Applications Society.